

Highly Enhanced Photoluminescence of Monolayer MoS₂ in Plasmonic Hybrids with Double-Layer Stacked Ag Nanoparticles

Ruhao Pan, Jianyu Kang, Yutong Li, Zhongshan Zhang, Renfei Li, and Yang Yang*

Cite This: <https://doi.org/10.1021/acsami.1c21960>

Read Online

ACCESS |



Metrics & More



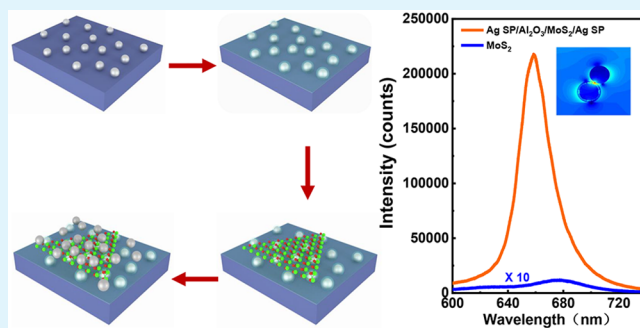
Article Recommendations



Supporting Information

ABSTRACT: In this work, a feasible method was proposed to prepare MoS₂-based plasmonic hybrid systems with high photoluminescence (PL) emission enhancement. The enhancement effect of plasmonic hybrids on the PL emission of MoS₂ has been systematically studied on MoS₂/Ag spherical nanoparticle (SP) hybrid systems with different architectures by changing the stacking position of Ag SPs. It is demonstrated that the sandwich-like hybrid composed of monolayer MoS₂ and dielectric Al₂O₃ layer between two layers of Ag SPs has the highest PL enhancement. Remarkably, after adding an Al₂O₃ layer under MoS₂, the PL intensity enhancement up to 209 times was achieved in the sandwich-like hybrid system. Compared with the hybrid with single-layer SPs, the sandwich-like hybrid system with double-layer Ag SPs exhibited an obvious blue shift as a result of the selective enhancement of the A⁰ exciton in MoS₂. These results demonstrate that MoS₂/Ag SP hybrid nanosystems have significant implications for sensing and photoelectronic devices.

KEYWORDS: MoS₂, plasmonic hybrid, enhanced photoluminescence, Al₂O₃ layer, localized surface plasmon resonance



1. INTRODUCTION

Molybdenum disulfide (MoS₂) is a representative member of the two-dimensional (2D) transition metal dichalcogenide (TMD) family, which has received plenty of research interests due to its striking physical properties and extensive applications.^{1,2} When the thickness of MoS₂ is reduced to a monolayer, its bandgap shifts from 1.29 to 1.9 eV, accompanied with an enhancement of the photoluminescence (PL) up to 10⁴,^{3,4} which promises the application in optoelectronic devices.^{4–7} In addition, the semiconducting property of MoS₂ enables the potential applications in biological sensing and photocatalytic devices.^{8–10}

However, the low absorption due to the atomic-thin thickness of 2D TMDs restricts their practical applications in devices.¹¹ It has been demonstrated that integrating TMDs with plasmonic nanoscale metals, including metallic nanoparticles (NPs) and nanostructures, is a novel strategy to broaden the application (improve the performance) of TMD-based devices.^{12,13} Owing to the extensive plasmonic light–matter interaction, the light-harvesting efficiency and optical response of TMDs are significantly enhanced, leading to the exceptional potential performances of optoelectronic devices.¹⁴ With the advancement of nanomaterial synthesis and the development of nanofabrication techniques, TMD-based plasmonic hybrids have witnessed extensive progress in the past years. Noble metal NPs, due to its fabrication feasibility, high yield, and diverse morphologies, have been widely utilized

to integrate with TMDs for fabricating plasmonic hybrids. Diefenbach et al. proposed a hybrid structure by decorating Au NPs on the surface of monolayer MoS₂, which promoted PL by 20-fold.¹⁵ In 2017, a hybrid framework with the PL enhancement of 200 times was built by transferring CVD-grown MoS₂ to Au NP arrays.¹⁶ Wu and coauthors proposed a gap-mode plasmon-enhanced PL mechanism, of which a PL enhancement of 110-fold was achieved after dispersing Ag shell-isolated nanoparticles (SHINs) on top of the monolayer MoS₂ transferred to the Au film.¹⁷ Moreover, MoS₂ plasmonic hybrid nanosystems have been employed in surface-enhanced Raman scattering (SERS) for the application in sensing devices.^{18,19}

In addition to the NPs synthesized through wet chemical methods, NPs created using physical deposition methods, owing to their feasibility in large area fabrication, were also employed to enhance the PL emission of TMDs.^{20–24} However, the PL enhancement for these reported hybrid heterostructures was not as high as that for the hybrids formed with chemically synthesized NPs. Therefore, probing a feasible

Received: November 12, 2021

Accepted: February 8, 2022

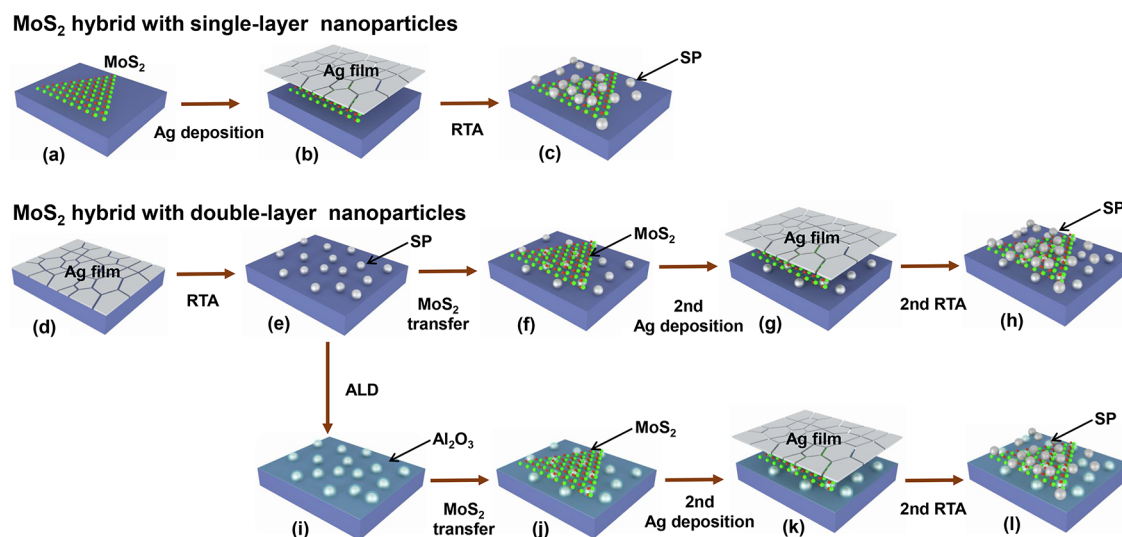


Figure 1. Schematic of the fabrication process for MoS₂/Ag SP plasmonic hybrids. (a) Monolayer MoS₂ transferred to a SiO₂/Si substrate. (b) Thin Ag film deposited by EBE on MoS₂. (c) Ag SPs produced on MoS₂ by the RTA process. (d) Thin Ag film deposited by EBE on a silicon wafer. (e) Ag SPs produced by the RTA process. (f) Monolayer MoS₂ transferred to Ag SPs. (g, h) Another thin Ag film deposited on Ag SP/MoS₂ followed by the RTA process to form a Ag SP/MoS₂/Ag SP hybrid nanostructure. (i, j) ALD process of coating a thin Al₂O₃ layer on the surface of Ag SPs and subsequent MoS₂ transfer. (k, l) Another thin Ag film deposited on Ag SP/Al₂O₃/MoS₂, followed by the RTA process to form a stacked hybrid structure of Ag SP/Al₂O₃/MoS₂/Ag SP.

method to prepare a plasmonic TMD hybrid with high PL enhancement is still an important issue for the fabrication and application of TMD-based optoelectronic devices.

According to previous reports, the PL enhancement of MoS₂ was closely related to the stacking sequences of MoS₂ and plasmonic nanoscale metals.²⁵ The sandwich-like three-layer hybrids possess higher PL-enhancing ability. However, to our knowledge, a three-layer plasmonic hybrid that is composed of TMDs and metallic NPs fabricated through physical deposition methods has not been reported.

In this work, the enhancement effect of plasmonic nanoparticles on the PL emission MoS₂ has been systematically studied on hybrids composed of Ag spherical nanoparticles (SPs) and MoS₂ with different architectures by designing the stacking position of Ag SPs. The sandwich-like structure formed by inserting monolayer MoS₂ and a dielectric Al₂O₃ layer between two layers of Ag SPs exhibited the highest PL enhancement of ~209-fold. Our work proposes a feasible method to prepare a MoS₂ hybrid nanostructure with high PL emission property, which promises the future applications in sensing and photoelectronic devices.

2. EXPERIMENTAL SECTION

2.1. Methodology. 2.1.1. Synthesis of Plasmonic Nanoparticles.

The fabrications of this plasmonic nanostructure need three kinds of processes: metal film deposition, rapid thermal annealing (RTA), and atomic layer deposition (ALD).²⁶ The Ag nanofilm was deposited by electron beam evaporation (EBE) on the cleaned SiO₂/Si substrates. The RTA technology was used to anneal the Ag nanofilms under the temperature of 350 °C for 3 min, and consequently, the surface morphology of the Ag nanofilm was changed from irregular nanoislands to spherical nanoparticles (SPs). A thin Al₂O₃ film was deposited separately on the as-formed Ag nanospheres by ALD under the temperature of 80 °C, and such a lower growth temperature was chosen to avoid the impact on the lower-layer Ag SPs.

2.1.2. Plasmonic Hybrid Preparation. Single-crystalline monolayer MoS₂ was grown through the chemical vapor deposition (CVD) process on a Si substrate with 90 nm SiO₂. In the fabrication procedure of the MoS₂/Ag SP hybrid structure, monolayer MoS₂ was

first removed from the SiO₂/Si substrate and transferred to the plasmonic substrates using a PMMA-assisted wet transfer procedure, which has been applied to transfer 2D materials.²⁷

2.1.3. Spectroscopy Experiments. PL and Raman measurements were carried out on a microconfocal Raman spectrometer (Horiba HR Evolution) equipped with an Olympus BX 41 microscope. A 100× (NA = 0.9) objective lens was used for focusing the laser on the sample surface and collecting the PL signal. The 532 nm laser was used as the excitation source for PL and Raman measurements, and the laser power on the sample was about 0.5 mW to prevent the overheating effect. The spectrum acquisition times were 30 and 10 s for Raman and PL acquisitions, respectively.

2.1.4. Numerical Simulation. To investigate the plasmonic enhancement effect of Ag nanoparticles on the PL emission of MoS₂, the finite-different time-domain (FDTD) method, which was a state-of-the-art method for solving Maxwell's equations in complex geometries,²⁶ was employed in this work to simulate the electric field distribution on different Ag SP nanostructures. The geometries of the SP nanostructures in the simulations were designed to match the SEM images. For simplicity, the spherical geometry was adopted for the Ag SPs. The diameter of Ag SPs was chosen as 30 nm, and the thickness of the Al₂O₃ layer was set to 3 nm. The wavelength of incident light was set at 532 nm and propagated along the z-axis. To be close to the experiment where the numbers of particles were illuminated by incident light, a unit cell with a 150 nm × 150 nm area in x–y was used. The source was a plane wave of 532 nm that was incidentally vertical to the SPs. The boundaries along x and y directions were periodic; however, 12 perfectly matched layers (PMLs) were used along the z-axis to avoid reflections. Also, all the mesh steps along the x-, y-, and z-axes are set to 0.5 nm to obtain accurate results of the field distribution in the SP nanostructures. The monitor was placed perpendicular to the y-axis to get a side view of field distribution.

3. RESULTS AND DISCUSSION

To systematically investigate the PL-enhancing capability of the plasmonic nanoparticles and MoS₂ hybrid systems, hybrid nanostructures with different architectures were designed and fabricated. Figure 1 shows a schematic of the fabrication procedures of different plasmonic hybrid nanosystems composed of Ag SPs and MoS₂ using RTA and ALD processes. Two kinds of hybrid architectures, MoS₂ coupled with single-

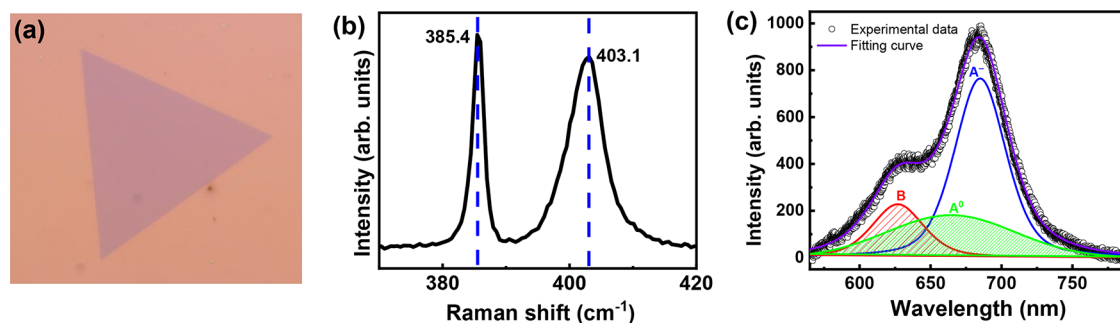


Figure 2. (a) Optical microscopy image, (b) Raman spectrum, and (c) PL spectrum of the bare monolayer MoS₂. The PL spectrum was deconvoluted into three peaks (A⁰ exciton (A⁰), trion (A⁻), and B exciton (B)) using Lorentzian curves.

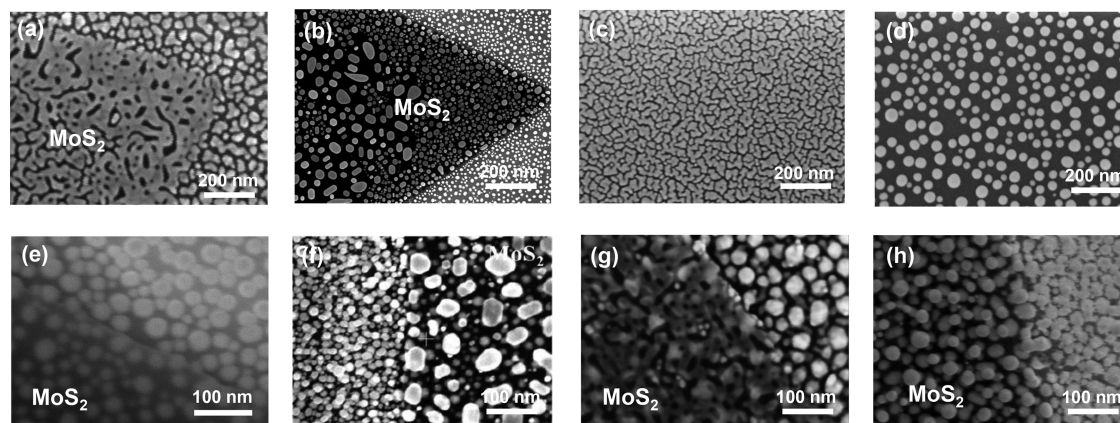


Figure 3. SEM images of different plasmonic hybrid samples. Five nanometer Ag film deposited on monolayer MoS₂ (a) before and (b) after RTA. Five nanometer Ag film deposited on the Si/SiO₂ substrate (c) before and (d) after RTA. (e) Monolayer MoS₂ transferred to Ag SPs. (f) Five nanometer Ag film deposited on Ag SP/MoS₂ after RTA. Ag film deposited on Ag SP/Al₂O₃/MoS₂ (g) before and (h) after RTA.

layer nanoparticles and double-layer nanoparticles, were proposed. First, monolayer MoS₂ is transferred to a SiO₂/Si substrate, as shown in Figure 1a. Then, as illustrated in Figure 1b, a 5 nm-thick Ag film (Ag-f) is deposited on monolayer MoS₂ using E-beam evaporation. After the RTA process, Ag SPs are created on the top of MoS₂, forming the MoS₂/Ag SP hybrid, as shown in Figure 1c.

For the hybrid of MoS₂ and double-layer Ag SPs, monolayer MoS₂ is sandwiched in between two layers of Ag SPs. In this case, a layer of Ag SPs is first prepared by RTA of a 5 nm-thick Ag film deposited on the silicon wafer, as illustrated in Figure 1d,e. Then, monolayer MoS₂ is transferred to Ag SPs to form the Ag SP/MoS₂ hybrid heterostructure, as exhibited in Figure 1f. Next, another 5 nm-thick Ag film is deposited on MoS₂, and the subsequent second RTA process is again carried out to form another layer of Ag NPs on the surface of MoS₂, as shown in Figure 1g,h. The obtained hybrids are named as Ag SP/MoS₂/Ag-f and Ag SP/MoS₂/Ag SP, respectively.

Furthermore, a uniform 3 nm-thick Al₂O₃ layer can be deposited using an ALD process on the first layer of Ag SPs in advance of transferring MoS₂, as presented in Figure 1i,j. Then, the second layer of Ag SPs is created on the surface of MoS₂ by depositing the Ag film, followed by the RTA process, as exhibited in Figure 1k,l, which shows hybrids defined as Ag SP/Al₂O₃/MoS₂/Ag-f and Ag SP/Al₂O₃/MoS₂/Ag SP, respectively.

The CVD-grown MoS₂ exhibited good crystalline quality and spectral properties. As shown in Figure 2a, a triangular-shape monolayer MoS₂ is clearly seen. Figure 2b presents the

Raman spectrum collected from the bare MoS₂, which resembles the typical features of MoS₂ reported previously. Two Raman peaks appear at approximately 385.4 and 403.1 cm⁻¹, originating from the lattice vibration of bulk MoS₂, which are identified as E' and A₁' modes, respectively.²⁸ It can be seen that the frequency difference between E' and A₁' modes is smaller than 20 cm⁻¹, demonstrating that it originates from a monolayer MoS₂.²⁹ The PL spectrum from the bare monolayer MoS₂ is shown in Figure 2c, which in fact is composed of three peaks after deconvolution. The intense 684 nm peak and the 635 nm shoulder peak are assigned as the trion A⁻ and B excitons, respectively. The weak broad peak at around 664 nm is called as the neutral A⁰ exciton. The A⁰ and B excitons correspond to the direct gap transition at the K point,^{30,31} of which the energy difference is due to the spin-orbital splitting of the valence band.³² The process of the negative trion A⁻ emission arises from the interaction of two electrons and one hole.^{33,34} As illustrated in Figure 1, the RTA process will be applied to create Ag SPs on the surface of MoS₂. Therefore, to check the annealing effect on the optical property of MoS₂, the PL spectrum was collected on a monolayer MoS₂ annealed at 350 °C. There is no obvious change in the line shape and intensity of the PL spectrum, suggesting that the RTA process does not affect the PL emission of MoS₂ (Figure S1). If there is any change in the PL spectra of MoS₂ hybrids, it should be related to the interaction between Ag SPs and MoS₂.

As shown in Figure 3a, the porous Ag film is deposited on monolayer MoS₂ flakes called MoS₂/Ag-f. In contrast, isolated nanoislands are on the area without MoS₂. After RTA at 350

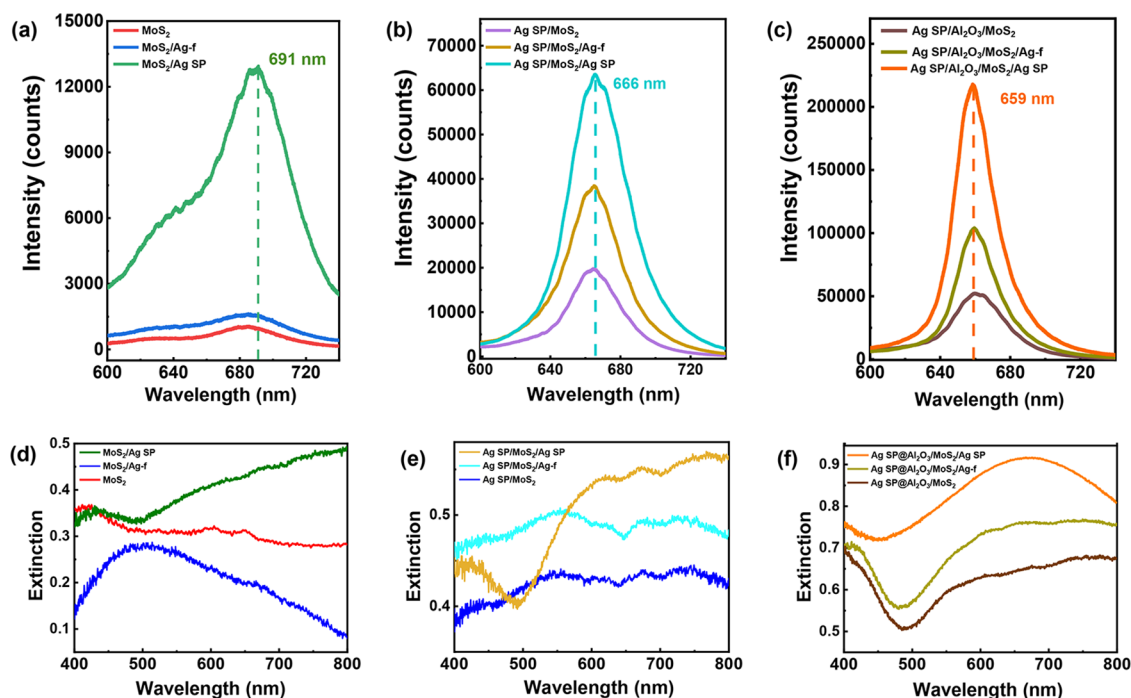


Figure 4. PL spectra and extinction spectra for the plasmonic hybrids of MoS₂. (a, d) Bare monolayer MoS₂ and 5 nm-thick Ag film deposited on MoS₂ before and after the RTA process, (b, e) MoS₂ transferred to Ag SPs and the Ag film deposited on Ag SP/MoS₂ before and after RTA process, and (c, f) MoS₂ transferred to Ag SP/Al₂O₃ and Ag deposited on Ag SP/Al₂O₃/MoS₂ before and after the RTA process.

°C in vacuum, Ag NPs are created on MoS₂, as exhibited in Figure 3b. Remarkably, the size of SPs is increasing from the edge to the center of MoS₂, which is larger than that formed on the bare substrate. For the sandwich-like plasmonic hybrid nanostructures, a 5 nm Ag film was first deposited on a SiO₂/Si substrate. The Ag film is not continuous, and randomly distributed cracks can be seen in Figure 3c. As exhibited in Figure 3d, Ag SPs with a size ranging from 30 to 50 nm were obtained after annealing. One can see that the SPs are not exactly in the sphere shape, some of which are a little ellipsoidal. Then, monolayer MoS₂ was transferred to Ag SPs, in which the boundary between the zones with and without MoS₂ can be seen clearly in Figure 3e. It is worth to note that nanoparticles with irregular shapes are formed on MoS₂ after the RTA process, as shown in Figure 3f. Notably, the size of Ag nanoparticles formed on MoS₂ is much larger than that created on the area without MoS₂.

For the sandwich-like MoS₂ hybrid nanosystem, monolayer MoS₂ was transferred to Ag SPs covered uniformly by a 3 nm-thick Al₂O₃ layer via the ALD process. As shown in Figure 3g,h, a porous Ag nanofilm and SPs are observed on MoS₂ after Ag deposition and RTA processes, respectively. Two layers of SPs can be seen clearly on both sides of the MoS₂ layer, as exhibited in Figure 3h. Remarkably, Ag SPs with uniform sizes can be achieved on MoS₂ buffered with Al₂O₃, which is in sharp contrast to that formed on MoS₂ without an Al₂O₃ layer (see Figure 3f).

Figure 4 presents the PL spectra collected from the plasmonic hybrids of MoS₂ illustrated in Figure 1. For each type of plasmonic hybrid, the spectra were collected on three different samples to check the repeatability of measurements (Figure S2). As shown in Figure 4a, the PL intensity is just increased a little after deposition of a 5 nm-thick Ag film on MoS₂, compared with bare MoS₂ (~1092 counts). Remarkably, the PL intensity is boosted to ~1.3 × 10⁴ counts, while

the Ag film transformed into Ag SPs after the RTA process. This prominent PL enhancement is attributed to the existence of Ag SPs, which gives rise to lots of localized surface plasmon resonance (LSPR) elements or so-called “hot spots”. It is worth to note that the PL emission center of MoS₂ shifted from 685 to 691 nm. The redshift of PL peaks can be attributed to the tensile strain-introduced reduction of the bandgap of MoS₂.^{35,36}

While exchanging the stacking sequences of Ag SPs and MoS₂, the PL intensity of MoS₂ is increased obviously. As exhibited in Figure 4b, the PL intensity of the Ag SP/MoS₂ hybrid heterostructure is up to ~2 × 10⁴ counts, which is increased 1.5 times compared with that of the MoS₂/Ag SP hybrid. Furthermore, after depositing a 5 nm-thick Ag film on MoS₂ (Ag SP/MoS₂/Ag-f), the PL intensity is further increased by 2-fold. After the RTA process, thus, the PL intensity is boosted to 6 × 10⁴ counts. It has been demonstrated that the electric field in the gap zone can be significantly enhanced while the gap width is narrow than 5 nm.³⁷ In the sandwich-like structure, a sub-1 nm nanogap structure was formed by placing MoS₂ in between the two-layer Ag SPs. Consequently, the PL emission is enhanced due to the extensively promoted LSPR.³⁸ The results shown in Figure 4b suggest that the sandwich-like hybrid nanostructure with double-layer Ag SPs holds a much higher PL enhancement effect than the two-layer hybrid structure with only single-layer Ag SPs. In addition, it is worthy to note that the peak position of the PL peak for the hybrids composed of Ag SPs covered by MoS₂ shifts to a shorter wavelength (~666 nm). The contribution from the coupling between the surface plasmons in Ag SPs and the exciton in MoS₂ plays an important role in the blue shift of the PL peak.^{16,27} Moreover, the compressive strain induced by the Ag SPs under the MoS₂ layer cannot be neglected.

It has been demonstrated that the dielectric layer can protect the plasmonic core from direct contact with analytes while allowing the transmission of an electromagnetic field from the core, promising further enhanced surface-enhanced Raman scattering (SERS) or surface-enhanced fluorescence (SEF).^{39,40} Therefore, it is predicted that the PL intensity would be further enhanced after depositing an Al₂O₃ layer on Ag SPs in advance of transferring MoS₂. As shown in Figure 4c, the PL intensity of MoS₂ transferred to 3 nm Al₂O₃ layer-coated Ag SPs (Ag SP/Al₂O₃/MoS₂) is promoted by 2.5 times compared to that of Ag SP/MoS₂. After depositing a 5 nm-thick Ag film on MoS₂, the PL intensity can be further doubled in Ag SP/Al₂O₃/MoS₂/Ag-f. Finally, the PL intensity is up to 2.2×10^5 counts after the RTA process, which is 2.2 times that before annealing. The PL intensity of the Ag SP/Al₂O₃/MoS₂/Ag SP hybrid is over three times that of the sandwich-like hybrid without an Al₂O₃ layer. To check the homogeneity of hybrid samples, PL mapping was performed on the surface of the Ag SP/Al₂O₃/MoS₂/Ag SP hybrid (Figure S3), in which the intensities for most points are comparable. The statistic of the intensity distribution over the scanning area exhibits nearly a Gaussian distribution. The area of the intensity in the range of $\pm 14\%$ of the central intensity covered 73.1% of the full scanning area (900 pixels). Remarkably, the PL intensity for Ag SP/Al₂O₃/MoS₂/Ag SP has been enhanced by over 200 times compared with that of bare MoS₂. A further blue shift (~ 659 nm) of the PL center was observed on the hybrids with an Al₂O₃ layer inserted between Ag SPs and MoS₂.

From the extinction spectra of these hybrids (Figure 4d–f), we can see that the strongest plasmonic resonant peak takes place on the Ag SP/Al₂O₃/MoS₂/Ag SP hybrid. Moreover, the broader resonant peak suggests that both the excitation field and spontaneous emission can be enhanced, which are responsible for the observed PL enhancement.

The density of Ag nanoparticles also plays an important role in the enhancement of PL. As we know, the thickness of the previously deposited Ag film is fixed. After annealing, the larger the particle size is, the fewer nanoparticles formed on MoS₂. We can see that the size of SPs in Figure 3h is much smaller than that of irregular nanoparticles in Figure 3f. Thus, the density of SPs is obviously higher than that of the irregular nanoparticles. Because the nanogaps are formed by the nanoparticles at the top and bottom of MoS₂ layer, the number of hot spots is increased with the higher density of SPs, leading to the further enhancement of PL intensity.

The PL enhancement factors (EFs) for these hybrid nanosystems discussed above are calculated by comparing their maximum intensity to that of the bare MoS₂. As illustrated in Figure 5, the PL EFs for the hybrid structure with one-layer SPs are much lower than those with double-layer stacked SPs. The EFs for MoS₂/Ag SP and Ag SP/MoS₂ are just about 12 and 19, respectively. For the case of the sandwich-like hybrid Ag SP/MoS₂/Ag SP, the PL EF is increased to 61 due to the sub-1 nm nanogaps created by SPs on two sides of MoS₂. Noticeably, the EF has been boosted by 209 times by depositing a dielectric Al₂O₃ layer on the top of the first layer Ag SPs.

In addition to the prominently enhanced PL emission, the line shapes of the PL spectra for these MoS₂ plasmonic hybrid nanostructures exhibit obvious differences. For the hybrid of MoS₂ underneath SPs (Figure S4a), its spectral line shape is similar to that of bare MoS₂ (Figure 2c). In contrast, the A⁰ exciton exhibits dominating enhancement in the MoS₂ hybrids

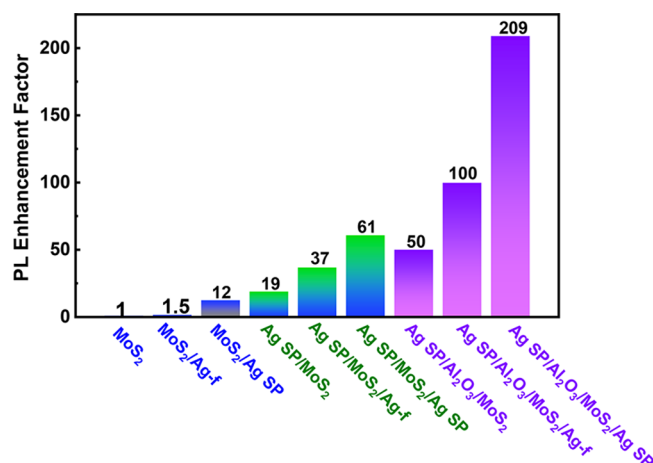


Figure 5. PL enhancement factor for different MoS₂ hybrids calculated using the PL intensity of bare MoS₂ as a reference.

with double-layer Ag SPs, as exhibited in Figure S4b,c. Therefore, as a result of the continuous enhancement of the A⁰ exciton, the maximum intensity of the PL emission for the plasmonic hybrids shifted from 684 to 659 nm (see Figure 4).^{41,42} Zeng and co-workers observed a blue shift of the PL peak of the hybrid constructed by transferring monolayer MoS₂ to Au NPs, which was attributed to the coupling of surface plasmon and exciton.¹⁶

Moreover, the remarkable enhancement of the A⁰ peak for the hybrids with double-layer Ag SPs observed in our work can be attributed to the p-doping of MoS₂ induced by thermal annealing.^{41,43} As reported in the previous literature, the trion recombination is dominant due to the excess electrons in the n-type MoS₂.^{44,45} During the RTA process for creating the second layer Ag SPs, depletion of S atoms occurred in the MoS₂ layer, resulting in an increased p-doping in MoS₂. Further, for the sandwich-like hybrid with the inserted Al₂O₃ layer, the charge exchange between MoS₂ and Al₂O₃ interfaces improved the conversion of the A⁻ trion into the neutral A⁰ exciton, resulting in the blue shift of the PL peak.^{42,46}

To get close insight into the plasmonic effect on the PL emission of MoS₂, the intensities of A⁰, B, and A⁻ components for different plasmonic hybrids are plotted in Figure 6a–c. We can see clearly that the intensity of all these three PL peaks continuously increased, while the hybrid structure evolved from single-layer SPs to double-layer SPs and then to double-layer SPs inserted with an Al₂O₃ layer. The results shown in Figure 6 confirmed our above discussion that the plasmon-exciton coupling effect plays an important role in the enhanced PL of these MoS₂ hybrids.

However, it is noticeable in Figure 6a–c that the intensity increasing rate for these hybrids differs much from each other. Then, the EFs for these three A⁰, B, and A⁻ emissions were calculated by dividing the intensities of their counterparts for the bare MoS₂. As exhibited in Figure 6d, the EF of the A⁰ exciton increased promptly compared with those of the B exciton and A⁻ trion. It is noteworthy that the A exciton is boosted by 1052 times, whereas the intensities of the B exciton and A⁻ trion for Ag SP/Al₂O₃/MoS₂/Ag SP are just enhanced by 42 and 54 times, respectively. Therefore, the promotion of the B exciton is not observed in Figure 4b,c, because the B peak becomes relatively weaker compared with the A⁰ peak.

The PL intensity from the MoS₂ hybridized with Ag SPs is determined by two processes: (i) excitation by the incident

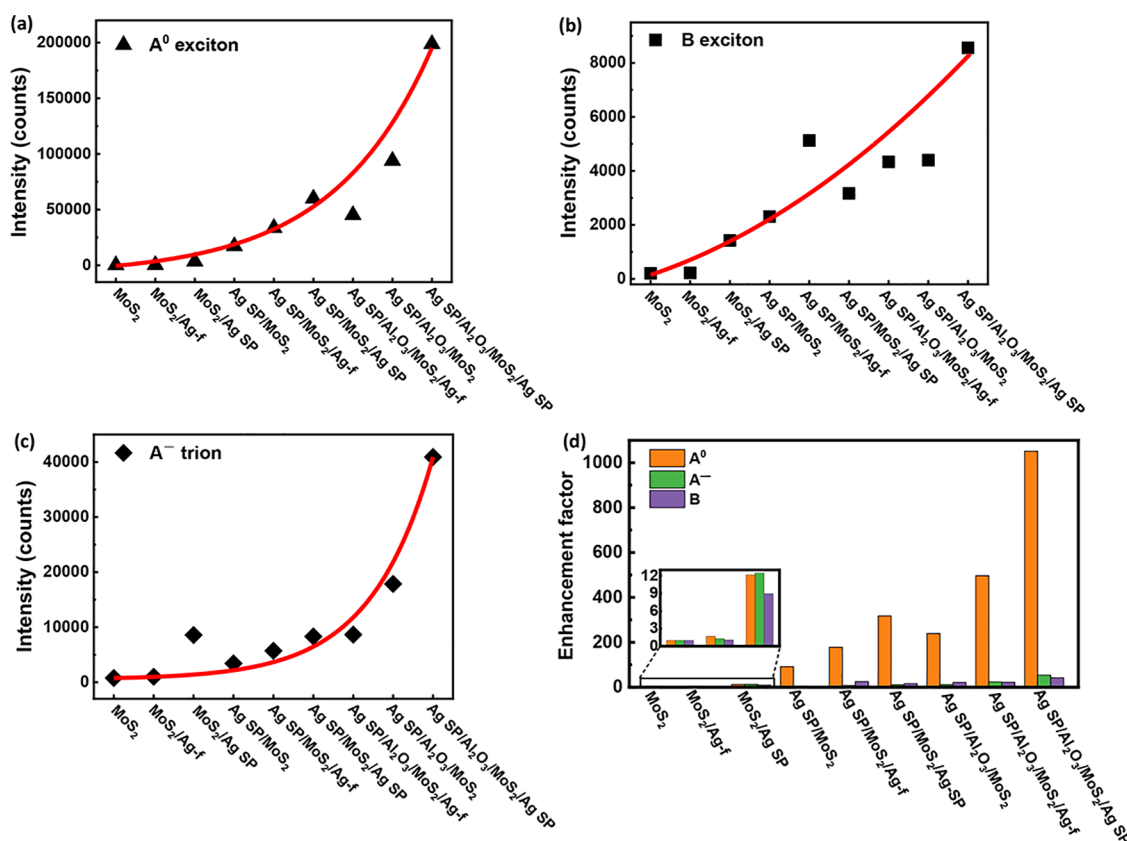


Figure 6. Peak intensity of (a) the A⁰ exciton, (b) B exciton, and (c) A⁻ trion for different MoS₂ hybrids. The red curves are the guide to the eyes. (d) Enhancement factor of the A⁰, B, and A⁻ peaks for different plasmonic hybrids calculated using the intensity of their counterparts for bare MoS₂ as a reference.

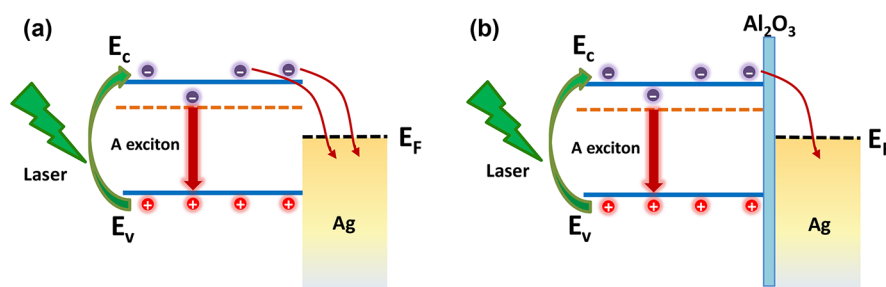


Figure 7. Schematic of the charge transfer for the MoS₂/Ag SP hybrids (a) without and (b) with an Al₂O₃ layer.

field, which is affected by the plasmonic nanostructures, and (ii) emission of radiation, which is influenced by the quenching effect due to the contact with Ag SPs.^{47,48} The enhanced PL intensity mainly benefits from the enhancement of excitation due to the strong LSPR, which is proportional to the square of the local electric field ($|E_{loc}|^2$). Obviously, the amplitude of hot spots in the hybrids with double-layer Ag SPs is higher than that in the hybrids with single-layer Ag SPs. For the Ag SP/MoS₂ hybrids, Ag SPs directly contact with MoS₂, and the excited carriers in the MoS₂ layer can transfer to Ag SPs under laser illumination, leaving holes and causing p-doping in MoS₂.⁴⁹ As shown in Figure 7a, some of the excited electrons transfer from MoS₂ to Ag, and they do not decay back to their initial ground state, leading to the reduced multiexciton formation and PL intensity.

On the other hand, as illustrated in Figure 7b, the dielectric Al₂O₃ layer acts as a barrier, which significantly hinders the charge transferring from MoS₂ to Ag SPs.⁵⁰ To get a better

screening effect, the thickness of the dielectric layer is normally a little thicker than that required for the optimized LSPR.^{51,52} Because the nonradiative relaxation is suppressed, the A⁰ exciton formation is promoted, leading to the PL enhancement of MoS₂.⁵³ As demonstrated in Figure 4c, the Al₂O₃ layer plays an important role in the enhanced PL of MoS₂ hybrid nanostructures.

To understand the role of the LSPR effect in the enhanced PL emission of the MoS₂-based hybrid nanostructure, FDTD simulation was employed to evaluate the electromagnetic field distribution on different Ag SPs nanostructures. Figure 8a,b exhibits the localized electric field enhancement $|E/E_0|$ on a bare Ag SP and a Ag SP coated with a 3 nm Al₂O₃ shell layer, respectively. E is the local electric field on the surface and E_0 is the incident electric field. One can see that the enhanced electric fields locate on two sides of Ag SP due to the surface charge distribution excited by incident light. It is notable that the highest field enhancement factor $|E/E_0|$ is doubled after

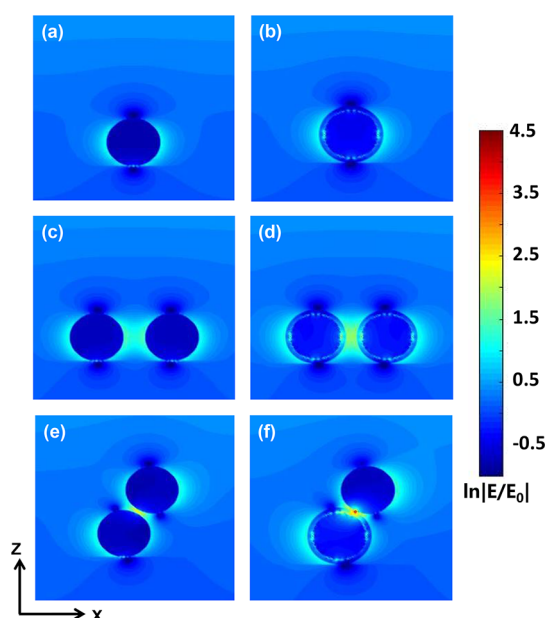


Figure 8. FDTD simulations showing the x - z view of electromagnetic field distribution of different Ag SP structures. (a) Bare Ag SP and (b) 3 nm Al_2O_3 shell layer-coated Ag SP. (c) Horizontal dimer composed of two bare Ag SPs. (d) Horizontal dimer composed of two Ag SPs coated with Al_2O_3 . (e) Vertical dimer composed of two bare Ag SPs. (f) Vertical dimer formed by stacking a bare Ag SP on an Al_2O_3 -coated Ag SP.

coating a dielectric Al_2O_3 layer on Ag SP, which takes place at the interface between the Al_2O_3 shell and the Ag SP core.

Then, the models of a dimer structure composed of two SPs with a 3 nm nanogap were built, as illustrated in Figure 8c,d, in which the highly intense “hot spot” appears at the nanogap between two Ag SPs. The enhancement factor $|E/E_0|$ is about 5, which is much higher than that on the single SP. Moreover, the enhancement factor $|E/E_0|$ for the dimer of Al_2O_3 -covered Ag SPs is nearly doubled compared with that on the dimer of Ag SPs. In the simulation model shown in Figure 8e, the width of the nanogap was set as 0.7 nm according to the thickness of the monolayer MoS_2 . According to the previous literature, if the width of the nanogap in the dimer is too small (<1 nm), the amplitude of the local electric field is reduced due to the quantum tunneling effect.⁵⁴ The dielectric layer with a high reflective index works as a spacer to form a thin nanogap (~ 3 nm) between two Ag SPs, which has a higher electric field intensity than that in the dimer formed by two bare Ag SPs. Using finite element method calculation, Zhai et al. demonstrated that the existence of the dielectric layer can reduce the loss of electric field enhancement by improving the light absorption efficiency.⁵⁵

As demonstrated in Figure 4, PL emission from the hybrid nanostructure with double-layer SPs is prominently higher than that of the hybrid nanostructure with single-layer SPs. Thus, a two-layer SP structure composed of two SPs stacked vertically in the xz -plane is built for simplicity, as shown in Figure 8e,f. It is noteworthy in Figure 8e that the highest field appears in the nanojunction between two bare Ag SPs, which is enhanced by 25 times. As illustrated in Figure 8f, an Al_2O_3 shell layer-coated Ag SP is placed at the bottom of the double-layer structure. The strong field is confined within the nanogaps outside the dielectric shell of SPs, of which the field enhancement factor is promoted to 50. This striking

higher electric field enhancement on the dimer with Al_2O_3 -covered Ag SP can be associated with the dimer geometry, in which two particles were stacked vertically.²⁶ While the thickness of the dielectric layer changes, the stacking geometry of the vertical dimer varies, and the plasmonic resonance center shifts correspondingly.⁵⁶ The extinction spectra for the plasmonic nanostructures (Figures S5) show good agreement with our numerical simulation and previous reports.

One can see clearly that two hot spots appear at the nanojunctions between bottom- and top-layer SPs, suggesting that the double-layer SP structures are very advantageous for the generation of a dense population of “hot spots”. In addition to the boosted LSPR effect, the quantum yield can be promoted after inserting a dielectric layer between the TMD layer and plasmonic nanostructures, which plays an important role in the enhancement of PL.⁵⁷ Further experimental studies are needed for exploring the optimal thickness to achieve the highest PL enhancement for this kind of plasmonic double-layer hybrid nanostructure.

As shown in Figure 4c, the PL peaks locate at about 666 nm. FDTD simulation was carried out on the vertical dimer under a 660 nm excitation wavelength to check the coupling between LSPR and emission. As exhibited in Figure S6, the highest electric field enhancement also appears at the nanojunction between two Ag SPs. Remarkably, the enhancement $|E/E_0|$ is about 15, much lower than that obtained under a 532 nm laser. This implies that selecting the excitation wavelength close to the resonance center promises a high efficiency for boosting the PL emission of the hybrid nanostructure proposed in this work.

4. CONCLUSIONS

In conclusion, we proposed a reproducible high-throughput nanofabrication technique to form a sandwich-like hybrid nanostructure composed of MoS_2 and double-layer stacking Ag SPs for highly enhanced PL emission of MoS_2 . The sandwich-like plasmonic hybrids exhibited the selective enhancement of the A^0 exciton of MoS_2 . The highest PL enhancement up to 209-fold occurred on the sandwich-like hybrid structure by introducing an Al_2O_3 layer under MoS_2 . The prominent PL enhancement can be attributed to the increased population of “hot spots” in the double-layer stacking Ag SP structure and the dielectric screen effect of the Al_2O_3 layer. Moreover, the remarkable blue shift of PL emission was observed in the sandwich-like hybrids, which can be attributed to the selective enhancement of the A^0 exciton. Our work provides a novel method to fabricate plasmonic hybrids with high PL enhancement ability, which has significant implications for sensing and photoelectronic devices.

ASSOCIATED CONTENT

Supporting Information

The Supporting Information is available free of charge at <https://pubs.acs.org/doi/10.1021/acsami.1c21960>.

PL spectra of monolayer MoS_2 grown on the Si/SiO₂ substrate before and after RTA; selected PL spectra collected on three plasmonic hybrid samples; PL mapping analysis of the Ag SP/ Al_2O_3 / MoS_2 /Ag SP hybrid; fitting results for the PL spectra of three plasmonic hybrids; extinction spectra for different plasmonic nanostructures; FDTD simulation result for a vertical dimer formed by stacking a bare Ag SP on an

Al₂O₃-coated Ag SP under the excitation of 660 nm
(PDF)

AUTHOR INFORMATION

Corresponding Author

Yang Yang – Beijing National Laboratory for Condensed Matter Physics, Institute of Physics, Chinese Academy of Sciences, Beijing 100190, China; orcid.org/0000-0003-3785-9233; Email: yang.yang@iphy.ac.cn

Authors

Ruhao Pan – Beijing National Laboratory for Condensed Matter Physics, Institute of Physics, Chinese Academy of Sciences, Beijing 100190, China; orcid.org/0000-0002-5573-2992

Jianyu Kang – Beijing National Laboratory for Condensed Matter Physics, Institute of Physics, Chinese Academy of Sciences, Beijing 100190, China

Yutong Li – College of Life Science and Technology, Beijing University of Chemical Technology, Beijing 100029, China

Zhongshan Zhang – Beijing National Laboratory for Condensed Matter Physics, Institute of Physics, Chinese Academy of Sciences, Beijing 100190, China

Renfei Li – Beijing National Laboratory for Condensed Matter Physics, Institute of Physics, Chinese Academy of Sciences, Beijing 100190, China

Complete contact information is available at:
<https://pubs.acs.org/10.1021/acsami.1c21960>

Notes

The authors declare no competing financial interest.

ACKNOWLEDGMENTS

This work was supported by the National Key Research and Development Program of China (grant nos. 2018YFB0703500 and 2016YFA0200800), the National Natural Science Foundation of China (grant nos. 62175253, 12074420, 11674387, 61905274, and 11704401), the Key Deployment Project of Centre for Ocean Mega-Research of Science, Chinese Academy of Science (COMS2020J03), and China Postdoctoral Science Foundation (grant no. 2020M670506).

REFERENCES

- (1) Wang, Q. H.; Kalantar-Zadeh, K.; Kis, A.; Coleman, J. N.; Strano, M. S. Electronics and Optoelectronics of Two-Dimensional Transition Metal Dichalcogenides. *Nat. Nanotechnol.* **2012**, *7*, 699–712.
- (2) Zhou, J.; Lin, J.; Huang, X.; Zhou, Y.; Chen, Y.; Xia, J.; Wang, H.; Xie, Y.; Yu, H.; Lei, J.; Wu, D.; Liu, F.; Fu, Q.; Zeng, Q.; Hsu, C.-H.; Yang, C.; Lu, L.; Yu, T.; Shen, Z.; Lin, H.; Yakobson, B. I.; Liu, Q.; Suenaga, K.; Liu, G.; Liu, Z. A Library of Atomically Thin Metal Chalcogenides. *Nature* **2018**, *556*, 355.
- (3) Mak, K. F.; Lee, C.; Hone, J.; Shan, J.; Heinz, T. F. Atomically Thin MoS₂: A New Direct-Gap Semiconductor. *Phys. Rev. Lett.* **2010**, *105*, 136805.
- (4) Zheng, W.; Jiang, Y.; Hu, X.; Li, H.; Zeng, Z.; Wang, X.; Pan, A. Light Emission Properties of 2D Transition Metal Dichalcogenides: Fundamentals and Applications. *Adv. Opt. Mater.* **2018**, *6*, 1800420.
- (5) Radisavljevic, B.; Radenovic, A.; Brivio, J.; Giacometti, V.; Kis, A. Single-Layer MoS₂ Transistors. *Nat. Nanotechnol.* **2011**, *6*, 147–150.
- (6) Huo, N.; Konstantatos, G. Recent Progress and Future Prospects of 2D-Based Photodetectors. *Adv. Mater.* **2018**, *30*, 1801164.

(7) Wang, G.; Zhang, Y.; You, C.; Liu, B.; Yang, Y.; Li, H.; Cui, A.; Liu, D.; Yan, H. Two Dimensional Materials Based Photodetectors. *Infrared Phys. Technol.* **2018**, *88*, 149–173.

(8) Yan, D.; Qiu, W.; Chen, X.; Liu, L.; Lai, Y.; Meng, Z.; Song, J.; Liu, Y.; Liu, X.-Y.; Zhan, D. Achieving High-Performance Surface-Enhanced Raman Scattering through One-Step Thermal Treatment of Bulk MoS₂. *J. Phys. Chem. C* **2018**, *122*, 14467–14473.

(9) Farimani, A. B.; Min, K.; Aluru, N. R. DNA Base Detection Using a Single-Layer MoS₂. *ACS Nano* **2014**, *8*, 7914–7922.

(10) Zhang, W.; Liao, X.; Pan, X.; Yan, M.; Li, Y.; Tian, X.; Zhao, Y.; Xu, L.; Mai, L. Superior Hydrogen Evolution Reaction Performance in 2H-MoS₂ to That of 1T Phase. *Small* **2019**, *15*, 1900964.

(11) Piper, J. R.; Fan, S. Broadband Absorption Enhancement in Solar Cells with an Atomically Thin Active Layer. *ACS Photonics* **2016**, *3*, 571–577.

(12) Cotrufo, M.; Sun, L. Y.; Choi, J. H.; Alu, A.; Li, X. Q. Enhancing Functionalities of Atomically Thin Semiconductors with Plasmonic Nanostructures. *NANO* **2019**, *8*, 577–598.

(13) Li, X.; Zhu, J.; Wei, B. Correction: Hybrid Nanostructures of Metal/Two-Dimensional Nanomaterials for Plasmon-Enhanced Applications. *Chem. Soc. Rev.* **2016**, *45*, 4032.

(14) Sriram, P.; Manikandan, A.; Chuang, F.-C.; Chueh, Y.-L. Hybridizing Plasmonic Materials with 2D-Transition Metal Dichalcogenides toward Functional Applications. *Small* **2020**, *16*, 1904271.

(15) Diefenbach, S.; Parzinger, E.; Kiemle, J.; Wierzbowski, J.; Funke, S.; Miller, B.; Csiki, R.; Thiesen, P.; Cattani-Scholz, A.; Wurstbauer, U.; Holleitner, A. W. Manifold Coupling Mechanisms of Transition Metal Dichalcogenides to Plasmonic Gold Nanoparticle Arrays. *J. Phys. Chem. C* **2018**, *122*, 9663–9670.

(16) Zeng, Y.; Li, X.; Chen, W.; Liao, J.; Lou, J.; Chen, Q. Highly Enhanced Photoluminescence of Monolayer MoS₂ with Self-Assembled Au Nanoparticle Arrays. *Adv. Mater. Interfaces* **2017**, *4*, 1700739.

(17) Wu, Z.-Q.; Yang, J.-L.; Manjunath, N. K.; Zhang, Y.-J.; Feng, S.-R.; Lu, Y.-H.; Wu, J.-H.; Zhao, W.-W.; Qiu, C.-Y.; Li, J.-F.; Lin, S.-S. Gap-Mode Surface-Plasmon-Enhanced Photoluminescence and Photoresponse of MoS₂. *Adv. Mater.* **2018**, *30*, 1706527.

(18) Chen, P. X.; Qiu, H. W.; Xu, S. C.; Liu, X. Y.; Li, Z.; Hu, L. T.; Li, C. H.; Guo, J.; Jiang, S. Z.; Huo, Y. Y. A Novel Surface-Enhanced Raman Spectroscopy Substrate Based on a Large Area of MoS₂ and Ag Nanoparticles Hybrid System. *Appl. Surf. Sci.* **2016**, *375*, 207–214.

(19) Li, J.; Zhang, W.; Lei, H.; Li, B. Ag Nanowire/Nanoparticle-Decorated MoS₂ Monolayers for Surface-Enhanced Raman Scattering Applications. *Nano Res.* **2018**, *11*, 2181–2189.

(20) Gong, L.; Zhang, Q.; Wang, L.; Wu, J.; Han, C.; Lei, B.; Chen, W.; Eda, G.; Goh, K. E. J.; Sow, C. H. Emergence of Photoluminescence on Bulk MoS₂ by Laser Thinning and Gold Particle Decoration. *Nano Res.* **2018**, *11*, 4574–4586.

(21) Zhao, W.; Wang, S.; Liu, B.; Verzhbitskiy, I.; Li, S.; Giustiniano, F.; Kozawa, D.; Loh, K. P.; Matsuda, K.; Okamoto, K.; Oulton, R. F.; Eda, G. Exciton-Plasmon Coupling and Electromagnetically Induced Transparency in Monolayer Semiconductors Hybridized with Ag Nanoparticles. *Adv. Mater.* **2016**, *28*, 2709–2715.

(22) Wang, F.; Xu, H.; Fang, J.; Wang, G.; Zhang, X. Probing the Interfacial Interaction between Monolayer Molybdenum Disulfide and Au Nanoclusters. *Surf. Interface Anal.* **2017**, *49*, 858–863.

(23) Zhang, D.; Wu, Y.-C.; Yang, M.; Liu, X.; Coileáin, C. Ó.; Abid, M.; Abid, M.; Wang, J.-J.; Shvets, I.; Xu, H.; Chun, B. S.; Liu, H.; Wu, H.-C. Surface Enhanced Raman Scattering of Monolayer MX₂ with Metallic Nano Particles. *Sci. Rep.* **2016**, *6*, 30320.

(24) Li, J.; Nie, C.; Sun, F.; Tang, L.; Zhang, Z.; Zhang, J.; Zhao, Y.; Shen, J.; Feng, S.; Shi, H.; Wei, X. Enhancement of the Photoresponse of Monolayer MoS₂ Photodetectors Induced by a Nanoparticle Grating. *ACS Appl. Mater. Interfaces* **2020**, *12*, 8429–8436.

(25) Yang, Y.; Liu, W. G.; Lin, Z. T.; Pan, R. H.; Gu, C. Z.; Li, J. J. Plasmonic Hybrids of Two-Dimensional Transition Metal Dichalcogenides and Nanoscale Metals: Architectures, Enhanced Optical Properties and Devices. *Mater. Today Phys.* **2021**, *17*, 100343.

- (26) Hu, Z.; Liu, Z.; Li, L.; Quan, B.; Li, Y.; Li, J.; Gu, C. Wafer-Scale Double-Layer Stacked Au/Al₂O₃@Au Nanosphere Structure with Tunable Nanospacing for Surface-Enhanced Raman Scattering. *Small* **2014**, *10*, 3933–3942.
- (27) Wang, Z.; Dong, Z.; Gu, Y.; Chang, Y.-H.; Zhang, L.; Li, L.-J.; Zhao, W.; Eda, G.; Zhang, W.; Grinblat, G.; Maier, S. A.; Yang, J. K. W.; Qiu, C.-W.; Wee, A. T. S. Giant Photoluminescence Enhancement in Tungsten-Diselenide-Gold Plasmonic Hybrid Structures. *Nat. Commun.* **2016**, *7*, 11283.
- (28) Zhang, X.; Tan, Q.-H.; Wu, J.-B.; Shi, W.; Tan, P.-H. Review on the Raman Spectroscopy of Different Types of Layered Materials. *Nanoscale* **2016**, *8*, 6435–6450.
- (29) Chakraborty, B.; Matte, H. S. S. R.; Sood, A. K.; Rao, C. N. R. Layer-Dependent Resonant Raman Scattering of a Few Layer MoS₂. *J. Raman Spectrosc.* **2013**, *44*, 92–96.
- (30) Splendiani, A.; Sun, L.; Zhang, Y.; Li, T.; Kim, J.; Chim, C.-Y.; Galli, G.; Wang, F. Emerging Photoluminescence in Monolayer MoS₂. *Nano Lett.* **2010**, *10*, 1271–1275.
- (31) Eda, G.; Yamaguchi, H.; Voiry, D.; Fujita, T.; Chen, M.; Chhowalla, M. Photoluminescence from Chemically Exfoliated MoS₂. *Nano Lett.* **2011**, *11*, 5111–5116.
- (32) Xiao, D.; Liu, G.-B.; Feng, W.; Xu, X.; Yao, W. Coupled Spin and Valley Physics in Monolayers of MoS₂ and Other Group-VI Dichalcogenides. *Phys. Rev. Lett.* **2012**, *108*, 196802.
- (33) Kim, H.; Yoon, Y. G.; Ko, H.; Kim, S. M.; Rho, H. Charge Transfer across Monolayer/Bilayer MoS₂ Lateral Interface and Its Influence on Exciton and Trion Characteristics. *2D Mater.* **2019**, *6*, No. 025004.
- (34) Pei, J.; Yang, J.; Yildirim, T.; Zhang, H.; Lu, Y. Many-Body Complexes in 2D Semiconductors. *Adv. Mater.* **2019**, *31*, 1706945.
- (35) Castellanos-Gomez, A.; Roldán, R.; Cappelluti, E.; Buscema, M.; Guinea, F.; van der Zant, H. S. J.; Steele, G. A. Local Strain Engineering in Atomically Thin MoS₂. *Nano Lett.* **2013**, *13*, 5361–5366.
- (36) Conley, H. J.; Wang, B.; Ziegler, J. I.; Haglund, R. F., Jr.; Pantelides, S. T.; Bolotin, K. I. Bandgap Engineering of Strained Monolayer and Bilayer MoS₂. *Nano Lett.* **2013**, *13*, 3626–3630.
- (37) Yang, Y.; Gu, C.; Li, J. Sub-5 nm Metal Nanogaps: Physical Properties, Fabrication Methods, and Device Applications. *Small* **2019**, *15*, 1804177.
- (38) Chen, W.; Zhang, S.; Kang, M.; Liu, W.; Ou, Z.; Li, Y.; Zhang, Y.; Guan, Z.; Xu, H. Probing the Limits of Plasmonic Enhancement Using a Two-Dimensional Atomic Crystal Probe. *Light Sci. Appl.* **2018**, *7*, 56.
- (39) Li, C. Y.; Yang, Z. W.; Dong, J. C.; Ganguly, T.; Li, J. F. Plasmon-Enhanced Spectroscopies with Shell-Isolated Nanoparticles. *Small* **2017**, *13*, 1601598.
- (40) Guerrero, A. R.; Aroca, R. F. Surface-Enhanced Fluorescence with Shell-Isolated Nanoparticles (SHINEF). *Angew. Chem., Int. Ed.* **2011**, *50*, 665–668.
- (41) Han, G. G. D.; Smith, B. D.; Xu, W.; Warner, J. H.; Grossman, J. C. Nanoporous Silicon-Assisted Patterning of Monolayer MoS₂ with Thermally Controlled Porosity: A Scalable Method for Diverse Applications. *ACS Appl. Nano Mater.* **2018**, *1*, 3548–3556.
- (42) Chen, F.; Wang, T.; Wang, L.; Ji, X.; Zhang, Q. Improved Light Emission of MoS₂ Monolayers by Constructing AlN/MoS₂ Core-Shell Nanowires. *J. Mater. Chem. C* **2017**, *5*, 10225–10230.
- (43) Nan, H.; Wang, Z.; Wang, W.; Liang, Z.; Lu, Y.; Chen, Q.; He, D.; Tan, P.; Miao, F.; Wang, X.; Wang, J.; Ni, Z. Strong Photoluminescence Enhancement of MoS₂ through Defect Engineering and Oxygen Bonding. *ACS Nano* **2014**, *8*, 5738–5745.
- (44) Mak, K. F.; He, K.; Lee, C.; Lee, G. H.; Hone, J.; Heinz, T. F.; Shan, J. Tightly Bound Trions in Monolayer MoS₂. *Nat. Mater.* **2013**, *12*, 207–211.
- (45) Lee, H. S.; Kim, M. S.; Kim, H.; Lee, Y. H. Identifying Multiexcitons in MoS₂ Monolayers at Room Temperature. *Phys. Rev. B* **2016**, *93*, 140409.
- (46) Kim, M. S.; Roy, S.; Lee, J.; Kim, B. G.; Kim, H.; Park, J. H.; Yun, S. J.; Han, G. H.; Leem, J. Y.; Kim, J. Enhanced Light Emission from Monolayer Semiconductors by Forming Heterostructures with ZnO Thin Films. *ACS Appl. Mater. Interfaces* **2016**, *8*, 28809–28815.
- (47) Aslan, K.; Lakowicz, J. R.; Szymanski, H.; Geddes, C. D. Metal-Enhanced Fluorescence Solution-Based Sensing Platform. *J. Fluoresc.* **2004**, *14*, 677–679.
- (48) Albella, P.; Moreno, F.; Saiz, J. M.; González, F. Surface Inspection by Monitoring Spectral Shifts of Localized Plasmon Resonances. *Opt. Express* **2008**, *16*, 12872–12879.
- (49) Bhanu, U.; Islam, M. R.; Tetard, L.; Khondaker, S. I. Photoluminescence Quenching in Gold-MoS₂ Hybrid Nanoflakes. *Sci. Rep.* **2014**, *4*, 5575.
- (50) Cheng, F.; Johnson, A. D.; Tsai, Y.; Su, P.-H.; Hu, S.; Ekerdt, J. G.; Shih, C.-K. Enhanced Photoluminescence of Monolayer WS₂ on Ag Films and Nanowire-WS₂-Film Composites. *ACS Photonics* **2017**, *4*, 1421–1430.
- (51) Song, B.; Jiang, Z.; Liu, Z.; Wang, Y.; Liu, F.; Cronin, S. B.; Yang, H.; Meng, D.; Chen, B.; Hu, P.; Schwartzberg, A. M.; Cabrini, S.; Haas, S.; Wu, W. Probing the Mechanisms of Strong Fluorescence Enhancement in Plasmonic Nanogaps with Sub-Nanometer Precision. *ACS Nano* **2020**, *14*, 14769–14778.
- (52) Reineck, P.; Gómez, D.; Ng, S. H.; Karg, M.; Bell, T.; Mulvaney, P.; Bach, U. Distance and Wavelength Dependent Quenching of Molecular Fluorescence by Au@SiO₂ Core-Shell Nanoparticles. *ACS Nano* **2013**, *7*, 6636–6648.
- (53) Kim, J. H.; Lee, H. S.; An, G. H.; Lee, J.; Oh, H. M.; Choi, J.; Lee, Y. H. Dielectric Nanowire Hybrids for Plasmon-Enhanced Light-Matter Interaction in 2D Semiconductors. *ACS Nano* **2020**, *14*, 11985–11994.
- (54) Zhu, W.; Esteban, R.; Borisov, A. G.; Baumberg, J. J.; Nordlander, P.; Lezec, H. J.; Aizpurua, J.; Crozier, K. B. Quantum Mechanical Effects in Plasmonic Structures with Subnanometre Gaps. *Nat. Commun.* **2016**, *7*, 11495.
- (55) Zhai, Y.; Deng, L.; Chen, Y.; Wang, N.; Huang, Y. Reducing the Loss of Electric Field Enhancement for Plasmonic Core-Shell Nanoparticle Dimers by High Refractive Index Dielectric Coating. *J. Phys.: Condens. Matter* **2020**, *32*, 105001.
- (56) Mühlhig, S.; Cialla, D.; Cunningham, A.; März, A.; Weber, K.; Bürgi, T.; Lederer, F.; Rockstuhl, C. Stacked and Tunable Large-Scale Plasmonic Nanoparticle Arrays for Surface-Enhanced Raman Spectroscopy. *J. Phys. Chem. C* **2014**, *118*, 10230–10237.
- (57) Chen, H.; Yang, J.; Rusak, E.; Straubel, J.; Guo, R.; Myint, Y. W.; Pei, J.; Decker, M.; Staude, I.; Rockstuhl, C.; Lu, Y.; Kivshar, Y. S.; Neshev, D. Manipulation of Photoluminescence of Two-Dimensional MoSe₂ by Gold Nanoantennas. *Sci. Rep.* **2016**, *6*, 22296.